A photometric redshift of $z \sim 9.4$ for GRB 090429B

A. Cucchiara[1,2,3], A. J. Levan[4], D. B. Fox[1], N. R. Tanvir[5], T. N. Ukwatta[6,7], E. Berger[8], T. Krühler[9,10], A. Küpcü Yoldaş[11,12], X. F. Wu[1,13], K. Toma[1], J. Greiner[9], F. Olivares E.[9], A. Rowlinson[5], L. Amati[14], T. Sakamoto[7] , K. Wiersema[5], K. Roth[15], A. Stephens[15], A. M. Soderberg[8], R. J. Foley[8], A. S. Fruchter[16], J.P.U. Fynbo[17], J. Hjorth[17], P. Jakobsson[18], P. T. O'Brien[5], J. Rhoads[19], R. E. Rutledge[20], M. A. Dopita[21], B. P. Schmidt[21], P. Podsiadlowski[22], R. Willingale[5] C. Wolf[22], S. R. Kulkarni[23]

cucchiara@astro.psu.edu

ABSTRACT

Gamma-ray bursts (GRBs) serve as powerful probes of the early Universe, with their luminous afterglows revealing the locations and physical properties of star forming galaxies at the highest redshifts, and potentially locating first generation (Pop III) stars. Since GRB afterglows have intrinsically very simple spectra, they allow robust redshifts from low signal to noise spectroscopy, or photometry. Here we present a photometric redshift of $z \sim 9.4$ for the *Swift* detected GRB 090429B based on deep observations with Gemini, the Very Large Telescope (VLT) and the GRB Optical and Near-infrared

[1]Department of Astronomy & Astrophysics, 525 Davey Laboratory, Pennsylvania State University, University Park, PA 16802, USA

[2]Lawrence Berkeley National Laboratory, M.S. 50-F, 1 Cyclotron Road, Berkeley, CA 94720

[3]Department of Astronomy, 601 Campbell Hall, University of California, Berkeley, CA 94720-3411

[4]Department of Physics, University of Warwick, Coventry, CV4 7AL, UK

[5]Department of Physics and Astronomy, University of Leicester, University Road, Leicester, LE1 7RH, UK

[6]Department of Physics, The George Washington University, Washington, D.C. 20052, USA

[7]NASA Goddard Space Flight Center, Greenbelt, MD 20771, USA

[8]Harvard-Smithsonian Center for Astrophysics, 60 Garden Street, Cambridge, MA 02138, USA

[9]Max-Planck-Institut für extraterrestrische Physik, Giessenbachstr. 1, 85740 Garching, Germany

[10]Universe Cluster, Technische Universität München, Boltzmannstraße 2, D-85748, Garching, Germany

[11]European Southern Observatory, Karl-Schwarzschild-Str. 2, 85748 Garching, Germany

[12]Institute of Astronomy, University of Cambridge, Madingley Road, CB3 0HA, Cambridge, UK

[13]Purple Mountain Observatory, Chinese Academy of Sciences, Nanjing 210008 (China)

[14]INAF - IASF Bologna, via P. Gobetti 101, 40129 Bologna (Italy)

[15]Gemini Observatory, 670 North A'ohoku Place, Hilo, HI 96720

[16]Space Telescope Science Institute, 3700 San Martin Drive, Baltimore, MD21218, USA

[17]Dark Cosmology Centre, Niels Bohr Institute, Copenhagen University, Juliane Maries Vej 30, 2100 Copenhagen O, Denmark

[18] Centre for Astrophysics and Cosmology, Science Institute, University of Iceland, Dunhagi 5, IS-107 Reykjavk, Iceland

[19]School of Earth & Space Exploration, Arizona State University, Box 871404, Tempe, AZ 85287-1404, USA

[20]Physics Department, McGill University, 3600 rue University, Montreal, QC H3A 2T8, Canada

[21]Research School of Astronomy & Astrophysics, The Australian National University, Cotter Road, Weston Creek ACT 2611, Australia

[22]Department of Physics, Oxford University, Keble Road, Oxford, OX1 3RH, UK

[23]Department of Astronomy, California Institute of Technology, MC 249-17, Pasadena, CA 91125, USA

Detector (GROND). The 90% likelihood range is $9.02 < z < 9.50$, and the lowest redshift allowed at 99% confidence is $z > 7.7$. The non-detection of the host galaxy to deep limits ($Y(AB) \sim 28$, which would correspond roughly to $0.001L^*$ at $z = 1$) in our late time optical and infrared observations with the *Hubble Space Telescope*, strongly supports the extreme redshift origin of GRB 090429B, since we would expect to have detected any low-z galaxy, even if it were highly dusty. Finally, the energetics of GRB 090429B are comparable to those of other GRBs, and suggest that the progenitor of GRB 090429B is not greatly different to those of lower redshift bursts.

Subject headings: galaxies: distances and redshifts - gamma rays: bursts - techniques: photometric

1. Introduction

The burst detections and rapid afterglow identifications of the *Swift* satellite (**?**), combined with intensive ground-based follow-up efforts, have confirmed some gamma-ray bursts (GRBs) as among the most distant objects known in the Universe (**??**), illuminating the conditions of star formation at the earliest epochs. As burst detections push towards progressively higher redshifts, the mere existence of GRBs at these times will provide important constraints on models of gravitational collapse, galaxy formation, and the early generations of stars. At the same time, high-quality spectroscopy of the burst afterglows can be expected to reveal element abundances (e.g. **???**), host galaxy kinematics, and potentially, the HI fraction of the intergalactic medium (IGM), as the process of cosmic reionization unfolds (e.g. **????**).

GRBs offer some advantages over other techniques for the selection and study of distant galaxies. Most notably, they have unprecedented luminosity, both of the prompt emission, and afterglow (e.g. **??**), enabling them to provide detailed diagnostics of their environments, and pinpointing their host galaxies however faint. However, this utility comes at a price – GRB afterglows achieve such brightness only fleetingly, and so the time available to obtain redshifts and other information for a burst is often very short (normally < 24 hours). In order to realize the ambitions of finding bursts at extreme redshift, and efficiently exploiting high-redshift GRBs as probes of this early cosmic epoch, it is necessary to devote increasing effort to the rapid identification of GRB near-infrared (NIR) afterglows. In addition to workhorse NIR instrumentation at large observatories, a growing number of dedicated facilities and instruments have been commissioned, with a primary aim of rapidly locating distant GRBs (e.g. PAIRITEL (**?**), GROND (**?**)). Followup spectroscopy of these candidates has proved several to be at very high redshift (e.g. **??**), culminating in GRB 090423 at $z \approx 8.2$ (**??**).

However, in some cases rapid spectroscopy is not possible, and we must fall back on photometric redshift measurements (e.g. **??**). Here again, GRBs offer some advantages over galaxies for the application of such techniques. Firstly, there is little intrinsic variation in the spectral shape of

an afterglow – it can be modelled simply as a power-law plus host galaxy extinction/absorption. This is in contrast to the diverse spectra of galaxies, which can have contributions from young/old populations (or a mixture), dust in complex configurations , exhibit intrinsic curvature, Balmer breaks etc, none of which are a concern for GRB afterglows. Secondly, the identity of a GRB afterglow is unambiguous from its fading, and thus there is no chance of mistaking a GRB afterglow with e.g. a Galactic L or T dwarf, which can also confuse high-z galaxy searches. It has been shown that GRB photometric redshifts are generally robust for these reasons (**?**). Indeed, while the fundamental accuracy is limited by the bandwidths and bands used, GRBs are much less subject to the catastrophic failure of photometric redshift determination, that can impact individual galaxy measurements.

In this paper we discuss the discovery and multi-wavelength followup of GRB 090429B. The afterglow was not visible in deep early optical imaging, but was found in deep IR observations starting $\sim$ 2.5 hours after the burst. While spectroscopic observations were curtailed by poor weather conditions, our photometry does allow us to construct a spectral energy distribution for the burst, and to infer a photometric redshift of $z \sim 9.4$, making GRB 090429B one of the most distant objects known to date.

The paper is structured as follows: in §**??** we present our full dataset on GRB 090429B and the uncertainties of our photometric measurements; in §**??** we derive our photometric redshift, supplemented with deep host observations. Finally, in Sec. **??** we summarize our conclusions, highlighting the importance rapid-response NIR imaging and spectroscopic capability on large telescopes for the study of the early Universe using GRBs. Throughout this paper we assume ΛCDM cosmology with $H_0 = 72$ km s^{-1} Mpc^{-1}, $\Omega_M = 0.27$, $\Omega_\Lambda = 0.73$, and use a standard nomenclature to describe the variation of the afterglow flux density as $F \propto t^{-\alpha}\nu^{-\beta}$.

2. Observations and Analysis

2.1. *Swift* observations

The Burst Alert Telescope (BAT; **?**) aboard the *Swift* satellite triggered on GRB 090429B at T_0 = 05:30:03 UT. The 15–350 keV light curve is composed of three distinct peaks with a total duration $T_{90} = 5.5$ s, and the time-integrated spectrum can be fitted by a single power-law with an exponential cut-off. The derived total fluence in the 15–150 keV band is 3.1×10^{-7}ergs cm^{-2}, with $E_{\rm peak} = 49$ keV. This peak energy is among the few detected by *Swift* within the BAT bandpass. Also, the lag analysis, obtained using the technique discussed in **?**, reveals that this GRB presents small spectral lags between the low-energy and the high-energy channels, which imply an isotropic luminosity $L_{iso} > 10^{52}$ erg/sec, not unusual for long GRBs.

After 106 s, the narrow-field instruments began their standard burst-response observation sequence. The X-ray Telescope (XRT; **?**) identified an uncataloged fading source at RA(J2000)=$14^{\rm h}02^{\rm m}40\overset{\rm s}{.}10$,

Dec(J2000)=+32°10′14.″6; no optical/UV counterpart was seen in the UV-Optical Telescope (UVOT; **?**) data. The X-ray data has been characterized using standard routines in HEASOFT, XSPEC, and QDP, with the light curve fitting process as described in **?**. For some analyses, we have used the automatic data products produced by the UK Swift Science Data Centre (**??**), our presentation of the *Swift* data quotes errors at the 90% level. The time-averaged 0.3–10 keV X-ray spectrum from 97–29893 seconds after the burst is best fit by a power-law with photon spectral index $\Gamma_{\rm X} = 2.01^{+0.16}_{-0.24}$ and with a total absorption column density of $N_{\rm H} = 10.1^{+4.6}_{-5.3} \times 10^{20}$ cm^{-2}, mildly (2.7σ) in excess of the Galactic absorption of 1.2×10^{20} cm^{-2}; we do not consider this discrepancy significant given the systematic uncertainties in the soft response of the XRT.

The X-ray light curve, given in Table **??** and illustrated in Figure **??**, is adequately fit by a combination of brightening and fading temporal power laws: initially, the X-ray flux rises with temporal index $\alpha_{\rm X1} = -0.96^{+0.43}_{-0.52}$, referenced to the burst time; following the peak time $T_{\rm X} = 589^{+146}_{-80}$ s, the light curve then breaks to a power-law decay with $\alpha_{\rm X2} = 1.20^{+0.08}_{-0.07}$.

2.2. Optical and Near-IR observations

Basic reduction steps for all optical and NIR photometry were performed using IRAF software[1]. Photometric analysis used both IRAF and the Starlink GAIA software, as well as our own custom scripts. Errors in the sky subtraction step are estimated from multiple apertures of size equal to that of the source aperture, placed around the field of the GRB.

Optical images were calibrated using field stars from the Sloan Digital Sky Survey (SDSS) Data-Release 7 (DR7) catalog (**?**) in the and NIR images were provisionally calibrated directly to the 2MASS catalog, but subsequently refined as described below. Detections and limits on the brightness of any associated source are presented in Table **??**.

2.2.1. ESO2.2m/GROND observations

The Gamma-Ray Burst Optical and Near-Infrared Detector (GROND, **?**) observed the field of GRB 090429B simultaneously in its (dichroic and filter defined) $g'r'i'z'JHK_s$ filter set beginning 14 minutes after the *Swift* discovery (**?**). No source was detected at the X-ray afterglow position in any of the seven bands: the limits being shallower than usual due to the high airmass for this (northern) field. Nonetheless, the implied X-ray to optical spectral slope of $\beta_{OX} < 0.1$ implied suppression of the optical flux relative to the X-ray, rendering GRB 090429B a "dark" burst under the definitions of **?** and **?**.

[1]IRAF is distributed by the National Optical Astronomy Observatories, which are operated by AURA, Inc., under cooperative agreement with NSF

2.2.2. VLT observations

Deep R and z-band observations were made with the VLT/FORS-2 camera at $\sim$60 minutes post-burst. Once again no optical source was visible at the position of the X-ray afterglow, confirming that it was unusually dark, and thus a good candidate high-z GRB (**?**).

2.2.3. Gemini-N observations

Beginning roughly 2.5 hours after the burst trigger, we carried out a series of observations from Gemini-North. We gathered optical $i'z'$ imaging with the Gemini Multi-Object Spectrograph (GMOS; **?**) and NIR JHK imaging with the Near-Infared Imager (NIRI; **?**). GMOS observations consisted of 5 exposures of 3 minutes each, per filter; NIRI observations consisted of 8 dithered positions of 60 s each. The Gemini GMOS and NIRI packages under the IRAF environment were used to sky-subtract, align, and combine the images. The NIRI images were also corrected for the small non-linearity effect seen in the detectors [2] Photometry was performed relative to SDSS stars for the GMOS data, and relative to secondary calibrators from GROND for the NIRI data (see §**??**). Our photometry is presented in Table **??**.

While no optical counterpart was present in our i' or z' images, we did identify a source within the X-ray localization in our NIR observations. The position of the source was RA=$14^{\rm h}02^{\rm m}40.10^{\rm s}$, Dec $=+32^\circ10\ '14\farcs20$. Following this discovery we attempted spectroscopic observations from Gemini-N, however, increasing summit winds forced the closure of the telescope and meant that these were aborted with <10 minutes of useable exposure time and no trace is visible in the observations. We obtained a second epoch of K-band observations on April 30 UT revealed a clear fading of $\approx$1.2 mag of the identified source, confirming its transient nature (and corresponding to a power-law index of $\alpha_K = 0.53 \pm 0.10$, shallower than the X-ray decay at that time). Figure **??** presents our Gemini imaging data, while the lower panel of Figure **??** shows our optical/NIR lightcurve. The resulting spectral energy distribution, from X-ray to IR is shown in Figure **??**.

No evidence of a host galaxy is present in our images. A deep r'-band image of the field, taken again with GMOS under good conditions ($0.4''$ seeing) at 14 days after the GRB, is shown in Figure **??**. This allows us to place a 3σ upper limit on the host galaxy apparent magnitude of $r' > 27.07$ mag. We also note in these images the presence of a massive elliptical galaxy, offset roughly $45''$ from the GRB location. This galaxy has absolute magnitude $M_r \approx -21.6$ and $M_K \approx -24.5$ ($\sim L^*$, **?**). It appears to be the central galaxy of a modest cluster at $z = 0.079$[3], It is likely that this foreground structure provides some lensing boost to the observed flux of the burst, although the relatively large impact parameter suggests it will not be a major factor.

[2] http://www.gemini.edu/sciops/instruments/niri/data-format-and-reduction/detector-linearization

[3] Redshift and r magnitude of galaxy obtained from the SDSS DR7 database; K magnitude from 2MASS.

2.2.4. HST observations

We obtained late time observations of the field of GRB 090429B with the *Hubble Space Telescope* (HST). These were taken after the afterglow had faded, and had the goal of finding or constraining the host galaxy. We used both the Advanced Camera for Surveys (ACS) and the Wide Field Camera 3 (WFC3). Observations were obtained in F606W (broad $V-R$), F105W (broad $Y-Z$) and F160W (H): a log of is shown in Table **??**. The data were reduced in the standard fashion using MULTIDRIZZLE and the *HST* archive "on-the-fly" calibration. All the images were drizzled to a common pixel scale of $0.05''$per pixel. We ascertained the location of the burst on the *HST* images via relative astrometry between our first epoch K-band observations, and those obtained with *HST*. Doing so we used a total of 11 and 10 sources in common to each frame, for ACS and WFC3 respectively. The resulting astrometric accuracy is $0\farcs08$ (F606W), $0\farcs07$ (F105W) and $0\farcs06$ (F160W) respectively. At the location of the afterglow we see no obvious host galaxy candidates in any of the images. To quantify the depths of these images we estimate the sky variance from a large number of background apertures ($\sim$50) placed in the field around the target position, avoiding visible sources. We then measure the resultant flux at the target position in an aperture of $0.4''$diameter, consistent with the approaches of many groups in searching for high-z galaxies (e.g. **??**). Our fluxes are shown in Table **??**. In addition to the measured fluxes we also show the effective AB-magnitude limits at these locations, which are equal to the measured flux density + 3σ, with an additional aperture correction to account for light missing within our small measurement apertures. These corrections are small for ACS (0.18 mag for F606W, **?**), but larger for the WFC3 images (0.31 and 0.54 magnitudes for F105W and F160W respectively [4]).

2.2.5. UKIRT observations

We obtained observations with the United Kingdom Infra Red Telescope (UKIRT), Wide Field Camera (WFCAM), beginning April 29 at 09:18 UT, roughly four hours post burst. Only a limited number of exposures were possible due to high wind keeping the telescope shut much of the night. These observations were not deep enough to reveal the afterglow, however because the large field of view (13.6 arcmin square for each chip) includes many bright 2MASS stars these images allowed us to precisely determine the magnitudes of fainter stars, which was crucial for calibrating the NIRI images (see §**??**). Pipeline reductions were performed by the Cambridge Astronomical Survey Unit (CASU[5]).

[4]http://www.stsci.edu/hst/wfc3/phot_zp_lbn

[5]http://casu.ast.cam.ac.uk/

2.3. Precise Photometric Calibration and Uncertainties

Since our photometric redshift analysis will depend critically on the accuracy of our photometry, we took particular care in both the calibration and estimates of photometric uncertainties.

The Gemini-N/NIRI detections are crucial, but also difficult to analyse since the field of view is small (2 arcmin on a side) and there is only one 2MASS star (namely star B in Table **??**, and Figure **??**) that is in all the sub-exposures of the 9-point dither pattern. There is another 2MASS star (A in Table **??**) which appears on two of the sub-exposures, and we used this as a double check on the derived photometry. Both these stars are towards the faint end of the 2MASS catalog and have relatively large photometric uncertainties. To overcome this we used the wide-field UKIRT/WFCAM and ESO2.2m/GROND JHK images (both of which were obtained close in time to the Gemini observations), which were very precisely calibrated using many bright 2MASS stars, to obtain more accurate magnitudes for these reference stars. The two independent determinations were consistent with each other within their respective calculated errors (typically 0.01–0.02 mag), and we therefore formed a weighted average to obtain our best estimates of the NIR magnitudes, as shown in Table **??**.

Magnitudes for the afterglow were measured relative to star B, although this procedure was further complicated by the fact that the point-spread-function (PSF) was found to change across the frame resulting in the core of the reference star becoming noticeably extended when it was close to the southern edge of the detector, as it was in some sub-exposures. This precluded small aperture (5 pixel radius, $\approx 0.6\ ''$) photometry for these exposures, so in such cases we used a fainter star (C in Table **??**) closer to the GRB position as a secondary reference, having determined its magnitude relative to star B using those frames where it was not near the edge. We note that a small aperture was required to maximise the signal-to-noise for the afterglow, and that profile-fitting photometry was deemed inappropriate due to the small number of bright stars available to define the PSF.

The magnitudes (and errors) for the afterglow in each band were then determined from an error weighted mean of the different sub-exposures. Finally we converted to flux density using a recent NIR spectrum of Vega (see **?**) which resulted in values that are 2–3% higher for our passbands than found using the conversion in table 7 of **?**. These are the flux densities reported in Table **??**, although we note that when we come to the photometric redshift analysis (below) we fit in counts rather than flux, to allow for the different spectral shapes of the afterglow and comparison star.

Since the optical observations provided only upper limits the overall fit is not strongly sensitive to the precision of the optical photometry. However, in this case, the field of GRB 090429B lies fortuitously within the SDSS survey area, and our most constraining optical limits (from GMOS) are obtained in the same filter set. This allows a precise photometric calibration of these images. For our VLT observations we calibrate the field using SDSS observations and the transforms of **?**. These latter values were confirmed as reasonable using archival zeropoints.

3. Results and Discussion

3.1. Temporal behaviour

Since our observations were taken over several hours, temporal variations in the afterglow luminosity could effect our analysis. Unfortunately we have rather little handle on the variability at optical/IR wavelengths. Although most GRB's begin power-law decline in luminosity fairly early, in some cases flat or even increasing luminosity can be seen for a period of time. A rapidly fading afterglow (similar to those commonly observed) would imply even more stringent upper limits in our (earlier) blue band filters since the extrapolation to a common time would yield a more extreme limit on colour index in e.g. $z - H$. Alternatively the more unusual case of a rapidly rising afterglow would yield somewhat weaker constraints since the non-detections in the bluer bands could be ascribed to the brightening of the afterglow in the time frame between the optical and IR observations. However, this is countered by the fact that such a rising afterglow would also imply an even bluer $H - K$ colour, more difficult to attain with extinction. In this scenario, the rising of the afterglow may offer some support for a high redshift scenario, since the time dilation at $z \sim 9$ would result in a forward shock which takes a factor of ~ 10 longer to reach maximum than at $z \sim 0$.

In an attempt to constrain the temporal slope of the optical afterglow we first perform photometry on the individual NIRI frames. We find no statistically significant variation over the ~ 10 minute time frame of these observations, implying that the afterglow is not varying especially rapidly. Secondly, we utilize acquisition images taken prior to the aborted NIRI spectroscopic observations. These suggest a minor brightening of the afterglow between 13000 s and 17000 s after the burst (0.3 ± 0.2 magnitudes, corresponding to $\alpha \approx -1.0 \pm 0.7$). However, these observations were obtained at a single dither position, and contained substantial persistence. Hence, we can accurately remove neither sky nor dark current and the resulting observations contain large variations in the sky on relatively short length scales. Thus, we caution against their use for detailed photometric work, aside from noting that suggest that the afterglow is neither rising, nor falling at an unusually rapid rate. We gain a much better handle on the decay between the first and second night observations, which gives $\alpha \approx 0.6 \pm 0.1$, but of course this may not apply during the first few hours post-burst.

On balance, then, we favor photometric fitting in which the observed magnitudes are assumed to be constant over the period of the early observations (i.e. we assume $\alpha = 0$). This is consistent with the relatively flat X-ray behaviour between one and three hours post burst (Figure **??**). For completeness, we have included a single power-law temporal decay as a possible parameter within these fits, and confirm that for any reasonable slope $-1 < \alpha < 1$ our results are broadly insensitive to the assumed value of α (see below). To avoid extrapolating over to wide a range of times, and the counter against any unusual afterglow behaviour (which is normally most notable at early times) we also fit *only* data taken after the 3000 s. The inclusion of early data strengthens our results if we assume that the afterglow is decaying, and makes a minimal contribution to the fit if we assume

$\alpha = 0$ (since the limits are shallower than those obtained at later times).

3.2. Photometric Redshift Analysis

Here we attempt to derive the redshift of GRB 090429B via our broadband photometry of its afterglow. The absence of any detections within the optical window, if interpreted as the signature of high redshift, immediately implies $z > 6.3$. Similarly, if we interpret the red $J - H$ colour of the afterglow as indicative of a Lyman-break lying within the J-band, the inferred redshift is $8.0 < z < 10.5$.

To obtain stronger constraints on the redshift of GRB 090429B we performed the following analysis. We considered just the seven deepest observations, namely those obtained at the VLT and Gemini-N on the first night. We assume initially there is no temporal variation over the course of observations, although including plausible variability within our fits also confirms that our results are broadly insensitive to this assumption (see below). After correcting for galactic foreground extinction ($E_{B-V} = 0.015$, **?**) we fitted these flux density measurements with a grid of simple models for the spectral energy distribution of the afterglow. The errors are likely to be Gaussian distributed, to good approximation, since the uncertainties are dominated by background-subtraction (although we also included zero-point calibration uncertainties in the modelling), and therefore used minimum-χ^2 fitting.

Specifically, the model was a simple power-law, with the spectral index, β_O, and overall normalisation as free parameters. The grid of models spanned a range in redshift of $0 < z < 12$ and rest-frame V-band extinction of $0 < A_V < 12$. Beyond $z \sim 7$ we are effectively fitting only three data points so there exists a degeneracy between extinction (A_V) and β_O. We therefore include a weak prior for the probability distribution of the value of β_O, (see Figure **??**) which is modelled as a log-normal with a peak likelihood at $\beta_O = 0.5$ and a width such that the relative likelihood is 50% of the maximum from about $0.3 < \beta_O < 0.85$. This is physically motivated since it allows values of β_O over a broad range, comparable to the range usually observed, but in particular prefers $\beta_O = \beta_X - 0.5 \approx 0.5$, as would be expected if there was a cooling break between the X-ray and optical regimes. The plausibility of such a cooling break is clear from Figure **??**, while relaxing this assumption does not lead to any viable fits at low redshift. Added to this was absorption due to neutral hydrogen in the intergalactic medium (**?**), (neutral hydrogen in the host was taken as a typical value of $10^{21}\,\mathrm{cm}^{-2}$, although the results are insensitive to the exact number assumed), and extinction due to dust. We experimented with several dust laws, from the Milky Way, Large Magellanic Cloud (LMC) and Small Magellanic Cloud (SMC) (**?**), as well as the extinction law of **?**.

We also impose a weak prior on the intrinsic luminosity of the optical afterglow (Figure **??**). Studies such as that of **?**, indicate that there is an upper envelope to the (broad) distribution of GRB optical afterglow luminosities. We therefore apply a prior which is flat below this envelope

and cuts off exponentially at brighter luminosities, although the cut-off is slow enough to allow a reasonable probability that the luminosity could be somewhat higher.

In fact, rather than fitting directly to the flux densities, we integrated our model spectra over response functions and compared the counts obtained by integrating an approximate spectrum of the comparison star. The response functions were obtained from the measured filter transmission curves, multiplied by a typical atmospheric absorption curve generated by ATRAN[6]. Going to these lengths effectively corrects for the small difference in the SED shape of the afterglow from the reference star, although again the conclusions are not greatly affected. In Figure **??** we show the photometric data points and the best fit model for the afterglow spectrum assuming that the afterglow did not evolve temporally during the first three hours (see below), and that the dust is similar to that in the Small Magellanic Cloud, which has frequently been found to be a good approximation to the dust laws along many other GRB sight lines. We also show the best fit low-z model, which is formally ruled out at high confidence. In Figure **??** we plot contours of χ^2 over a grid of models spanning a range of redshift and rest-frame V-band extinction, A_V. The red-cross shows the best fitting model, which has $z = 9.36$ and extinction $A_V = 0.1$, although the 99% confidence contour runs as low as $z \approx 7.7$ if there is a modest amount of dust (rest-$A_V \sim 0.5$) in the host. Marginalising the likelihood over A_V (assuming a flat prior) indicates a 90% likelihood range of $9.02 < z < 9.50$. There is no solution at lower redshifts ($z < 7$) which is not ruled out at >>99.9% level: and the best fit at low redshift ($z \approx 0$ as it happens, as shown by the blue cross) requires very high extinction of $A_V \approx 10$.

In Figure **??** we show the likelihood contours for fits over a range of prior assumptions for the temporal power-law decline index α and dust law. Changing α to ± 1 makes rather little difference, and in any case, as discussed above, there is evidence to suggest the luminosity was not changing even as rapidly as this. Other dust laws do have more effect, largely due to the 2175 Å feature in the Milky-Way, LMC (**?**) and **?** laws producing the blue $H - K$ colour even at slightly lower redshifts, although generally speaking the best fit remains $z > 9$. The **?** dust-law was determined from observations of a quasar at $z = 6.2$ and is argued to consistent with dust produced largely from early supernovae (note that this law is only defined up to ~ 3200 Å in the rest frame, and we therefore graft it to the SMC law at this point). This case is interesting as it does allow redshifts as low as $z \sim 6.5$ at 99% confidence, although to date, only GRB 071025, with a photo-$z \sim 5$, has shown strong evidence of requiring such a dust law (**?**).

3.3. Implications of the absence of a host galaxy

Our late time date taken with Gemini and *HST* are potentially extremely valuable, since we can use the absence of any host galaxy candidates to assess the plausibility of any lower-z solutions

[6]http://atran.sofia.usra.edu/cgi-bin/atran/atran.cgi

to our photometric redshifts (the *HST* images are shown in Figure **??**). The detection of a host galaxy in the optical was used, for example, to show that GRB 060923A was $z < 3$ despite its afterglow being a K-band drop-out (**?**). In the case of GRB 090429B, the possible low-redshift scenarios seem to be those with $z < 1$ and high extinction (although emphasise that this remains a very significantly worse fit that our higher redshift scenario). The limits these data provide on this are shown graphically in Figure **??**, where we plot the absolute inferred magnitude of the host galaxy in the observed V, Y and H bands as a function of redshift. For completeness we cut each line at the point where 1216Å$\times(1 + z)$ passes the central wavelength of the band. At $z = 0.1$ close to the minimum of our lower redshift solution we obtain inferred absolute magnitude limits of $M_V > -10.6$, $M_Y > -9.9$, $M_H > -10.5$, these exceptionally deep limits are comparable to the luminosities of bright globular clusters, and significantly fainter than any known GRB or supernova host galaxy, indeed they place limits of $\leq 10^{-4}$ L^* (**?**). Even at $z = 1$ the observed Y-band limits would imply $M_B > -15.1$, or $\leq 0.001L^*$ (**?**).

In this regard it is worth noting that the lower redshift solutions are only viable in cases where the host galaxy extinction is high, whereas such faint galaxies typically have low metallicity, and little dust, and it is therefore extremely unlikely that one could create the extinction ($A_V \sim 10$) necessary to explain GRB 090429B. Any $z < 3$ solution would require the host of GRB 090429B to be fainter than the large majority of GRB hosts currently known. Furthermore, our wide wavelength coverage would also allow us to uncover any very red dusty host galaxies, which would provide the necessary extinction, but would be missing from optical only searches (e.g. **?**, Svensson et al. 2011, submitted).

This offers strong support for our high$-z$ model, In these cases only the F160W observation yields potential information as to the magnitude of the host galaxy. The inferred 1500 Å absolute AB magnitude at $z \sim 9.4$ is -19.95. This lies roughly in the middle of the observed absolute magnitude distribution of $z \sim 8$ candidate galaxies found in deep *HST* ACS and WFC3 imaging (**?**), and thus the non-detection of a galaxy at $z \sim 9.4$ is not unexpected in observations of this depth.

3.4. Other indicators of high redshift

In addition to the above discussion there are additional lines of evidence which offer support for the high$-z$ interpretation of GRB 090429B. The best very low redshift solution (which is a very poor fit to the available optical data) requires $A_V \sim 10$, for an SMC extinction law (e.g. **?**), which would correspond to a foreground $N_H \sim 10^{23}$ cm^{-2}, nearly two orders of magnitude larger than is observed. While the dust to gas ratios observed through the Milky Way, can show moderately large variations, such a large offset would be unheard of, particularly in GRB afterglows where typically the ratio of dust extinction to X-ray determined gas column is actually less than is seen locally (**?**). Hence the observed X-ray spectrum seems to rule out any low redshift ($z \lesssim 1$), high extinction scenario. This is illustrated if Figure **??** which shows that the best low-redshift solutions are well

above the contours of A_V inferred from the excess N_H assuming a typical GRB dust-to-gas ratio.

A second line of evidence comes from observed high energy correlations seen in many GRBs. In particular the relation between the peak energy of the νF_ν spectrum (E_p) and the burst isotropic energy (**?**). Although this relation has a significant scatter, it can also be used to place some constraints on the burst redshift under the assumption that all long bursts should follow the relation. For GRB 090429B, the burst is only consistent with this relation at better than 3σ if $z > 1$, implying that it also disfavours very low redshift models for the origin of GRB 090429B. This result couples with the Lag-luminosity relation, which would imply an isotropic luminosity of $L_{iso} \sim 10^{53}$ erg/sec, similar to other long GRBs in the "silver sample" (**?**).

3.5. Rest frame properties

The observed fluence of GRB 090429B is 3.1×10^{-7}ergs cm^{-2}, comparable to that observed for GRB 090423, and, for $z = 9.36$ implies an isotropic energy release in the 15-150 keV band of $E_{iso} = 3.5 \times 10^{52}$ ergs at $z \sim 9.4$. Its absolute X-ray brightness at ~ 1000 s of $\sim 2 \times 10^{49}$ ergs s^{-1}, and K-band luminosity of $M_{\lambda/(1+z)}$ of ~ -26.2(AB) are also similar both to GRB 090423 and the bulk of the long GRB population.

The rest-frame duration at first sight seems surprisingly short, with $T_{90}/(1+z) \sim 0.5$ s. Interestingly, three of the four highest redshift GRBs discovered prior to this one have also had rather low values of $T_{90}/(1+z)$ around 1–4 s (**???**). A possible explanation for this tendency may be that for high redshift sources the BAT is observing at rest frame MeV energies, where the light curves tend to be more rapidly variable and shorter duration than at lower energies, and thus it is plausible that just a single peak of emission is rising up above the noise in these cases.

Another interesting issue is that of the absorption inferred from the X-ray spectrum. Although the measurement is not highly significant, if taken at face value, the rest-frame column density is $N_H = 1.4^{+1.0}_{-1.0} \times 10^{23}\,\mathrm{cm}^{-2}$ (90% confidence range). This would be already high compared to most other *Swift* observed GRBs, and would be higher still if, as is very likely, the metallicity is substantially less than Solar (which by convention is often assumed in calculating N_H). Such a high column density is no doubt surprising, although a similar value was found for GRB 090423. As in that case, it also raises the question of whether a high gas column would be compatible with the low extinction indicated by the NIR afterglow. GRBs are expected to be able to destroy dust to fairly large distances from their birth sites (e.g. **??**), but the good fit for many afterglow SEDs with a SMC extinction law suggests they have not generally been highly modified by dust destruction, which would tend to produce "gray" extinction laws (e.g. **?**). Nonetheless, the large uncertainty on this measurement, and the wide range of dust to gas ratios seen to other GRB sight-lines, makes the significance of this conflict hard to assess.

On balance, it seems that in most respects the general properties of GRB 090429B do not stand far apart from the population of long GRBs, even at the inferred redshift of $z \sim 9.4$. In

particular it shows no evidence that its progenitor is distinct from those of GRBs seen in the more local Universe. This is of particular importance at $z \sim 9.4$, since it is close to the redshift where WMAP observations imply the bulk of reionization of the Universe occurred ($z = 10.6 \pm 1.2$, **?**). This reionization process is likely to have been driven by the first generations of star formation, including population III whose pristine H+He composition is expected to lead to generally more massive stars. It has been proposed that a consequence of this could be that population III stars produce particularly long duration, and energetic GRBs (e.g. **?**). This is clearly not the case for GRB 090429B, and hence we conclude that its progenitor was more likely to be a high-mass second generation (pop II) star.

4. Conclusions

We have presented our discovery and multi-wavelength observations of GRB 090429B and its NIR afterglow, and a deep late-time search for its host galaxy. The afterglow exhibited a strong spectral break in the J-band, which coupled with the non-detection in the optical, and relatively blue $H - K$ colour, allows us to derive a best fit photometric redshift of $z \sim 9.4$. It is, of course, important to look carefully at the evidence against a lower redshift origin, since we know that *Swift* GRBs exist in much greater number at $z < 4$ than above it. Our afterglow photometry allows us to exclude all low-z solutions with high confidence, with only solutions at $z > 7.7$ allowed at better than 99% confidence. The maximum-likelihood solution, with our preferred assumptions of a flat afterglow light curve over the course of our early observations (i.e. $\alpha = 0$) and an SMC extinction law, is $z = 9.36$ with a 90% likelihood range of $9.02 < z < 9.50$. The conclusions do not depend sensitively on these assumptions or the priors adopted for other parameters. A low redshift is also effectively ruled out by our *HST* observations which would easily locate such dusty galaxies in either the optical or IR at $z < 1$, and also the relatively modest excess N_H which would not be consistent with a high dust column.

This immediately implies that GRB 090429B is one of the most distant objects yet discovered. Small levels of extinction over the redshift range $7.5 < z < 9$ could reproduce the observed colours, although all $z > 6$ bursts observed to date are consistent with $A_V = 0$ (**??**), suggesting that $z \sim 9.4$ provides a good estimate of the redshift of GRB 090429B.

Our campaign shows again how rapid-response multiband NIR observations play a crucial role in identifying candidate extreme-redshift afterglows. However, it also highlights the need for even more rapid observations and decisions to maximize the likelihood that spectroscopic observations can be successfully obtained. In the future, additional dedicated ground-based optical/NIR multi-band imagers such as GROND and RATIR (**?**) can be expected to feed further such candidates directly to NIR spectrographs including X-Shooter on the VLT (**?**), FIRE on Magellan (**?**), and GNIRS on Gemini (**?**); ultimately, such prompt spectroscopy of extreme-redshift candidates will not only resolve the nature of these events, but quite likely succeed in realizing the extraordinary promise of GRBs as probes of the extreme-redshift Universe.

The Gemini data, acquired under the program ID GN-2009A-Q-26, are based on observations obtained at the Gemini Observatory, which is operated by the Association of Universities for Research in Astronomy, Inc., under a cooperative agreement with the NSF on behalf of the Gemini partnership: the National Science Foundation (United States), the Science and Technology Facilities Council (United Kingdom), the National Research Council (Canada), CONICYT (Chile), the Australian Research Council (Australia), Ministério da Ciência e Tecnologia (Brazil) and Ministerio de Ciencia, Tecnología e Innovación Productiva (Argentina). Based on observations made with the NASA/ESA Hubble Space Telescope, obtained from the data archive at the Space Telescope Institute. STScI is operated by the association of Universities for Research in Astronomy, Inc. under the NASA contract NAS 5-26555. Data presented in this paper is associated with programme GO-11189. Part of the funding for GROND (both hardware as well as personnel) was generously granted from the Leibniz-Prize to Prof. G. Hasinger (DFG grant HA 1850/28-1). TK acknowledges support by the DFG cluster of excellence "Origin and Structure of the Universe". AR acknowledges funding from the Science and Technology Funding Council. The Dark Cosmology Center is funded by the Danish National Research Foundation. FOE acknowledges funding of his Ph.D. through the *Deutscher Akademischer Austausch-Dienst* (DAAD).

We thank Paul Hewett for helpful discussions about absolute infrared flux calibration.

Table 1. Secondary standards within the NIRI field of view

Star	RA	DEC	J_{2MASS}	J_{cal}	H_{2MASS}	H_{cal}	K_{2MASS}	K_{cal}
A	14:02:35.05	32:11:07.2	14.754	14.753	14.411	14.407	14.212	14.341
			±0.034	±0.006	±0.055	±0.008	±0.075	±0.010
B	14:02:40.60	32:09:28.9	15.419	15.451	14.968	15.023	14.846	14.944
			±0.055	±0.007	±0.076	±0.009	±0.127	±0.015
C	14:02:38.11	32:10:08.9		19.523		19.001		18.585
				±0.035		±0.028		±0.032

Note. — Vega magnitudes for our two secondary standard stars utilized in photometry of the afterglow of GRB 090429B. The $2MASS$ entries refer to the magnitudes contained within the 2MASS catalog, while those denoted *cal* refer to our improved values based on the UKIRT/WFCAM and ESO2.2/GROND observations. Uncertainties are 1σ.

Table 2. X-ray Observations

T-T_0 (s)	Flux density (μJy)	Error (μJy)
158	0.53	0.12
291	0.80	0.18
368	1.18	0.27
452	1.19	0.27
561	1.69	0.36
651	1.37	0.31
708	1.35	0.30
768	1.18	0.27
838	1.00	0.22
927	1.31	0.21
4618	0.099	0.026
5636	0.111	0.029
6417	0.126	0.033
10316	0.089	0.023
10982	0.087	0.023
15921	0.0269	0.0053
120249	0.0021	0.0006

Note. — X-ray observations obtained by the XRT instrument onboard the *Swift* satellite. The flux density is calculated at 2 keV, while the conversion factor from flux to Jy is 8.87×10^4 erg cm^{-2} s^{-1} Jy^{-1} (0.3–10 keV). The counts to flux conversion factor is 2.984×10^{-11} erg cm^{-2} s^{-1} counts^{-1}. Uncertainties are 1σ. For the best fit X-ray spectrum parameters see Sec. **??**.

Table 3. Log of ground-based optical/NIR Observations

T-T_0 (s)	Magnitude	Flux density (μJy)	Filter	Telescope
990	> 23.08		g'	GROND
990	> 22.86		r'	GROND
990	> 22.03		i'	GROND
990	> 21.87		z'	GROND
990	> 21.06		J	GROND
990	> 20.50		H	GROND
990	> 19.84		K	GROND
3224	> 24.5	0.00 ± 0.20	B	VLT/FORS2
4017	> 25.9	-0.08 ± 0.08	R	VLT/FORS2
5144	> 23.6	0.27 ± 0.34	z	VLT/FORS2
8135	> 25.7	0.02 ± 0.06	i'	Gemini-N/GMOS
9350	> 24.5	0.02 ± 0.18	z'	Gemini-N/GMOS
10611	22.80 ± 0.16	2.82 ± 0.44	J	Gemini-N/NIRI
11785	21.41 ± 0.05	10.21 ± 0.50	H	Gemini-N/NIRI
13280	21.12 ± 0.04	13.26 ± 0.51	K	Gemini-N/NIRI
95658	22.42 ± 0.16	4.0 ± 0.6	K	Gemini-N/NIRI
1.2×10^6	> 27.07		r'	Gemini-N/GMOS

Note. — Optical/NIR observations of GRB 090429B. Magnitudes are quoted in the AB system, and corrected for the expected Galactic extinction along the line of sight, $E_{B-V} = 0.015$. Quoted errors are 1σ and limits are the at 3σ level.

Table 4: Log of *HST* observations of the GRB 090429B field

Date	Start Time	Inst/Filter	Exp time	Limit	Flux density (μJy)
3 Jan 2010	03:13	ACS/F606W	2100	> 27.6	0.005 ± 0.008
10 Jan 2010	21:54	WFC3/F160W	2412		
22 Feb 2010	19:22	WFC3/F160W	2412	> 27.5	0.007 ± 0.005
24 Feb 2010	03:19	WFC3/F105W	2412		
28 Feb 2010	13:56	WFC3/F105W	2412	> 28.3	-0.001 ± 0.005

Note. — A log of the HST optical and NIR observations of the GRB 090429B field. Flux densities are given in the measured apertures and are not corrected for light outside the apertures. Errors are 1σ and the limits are given in the AB-magnitude system at the 3σ level (and do include aperture corrections).

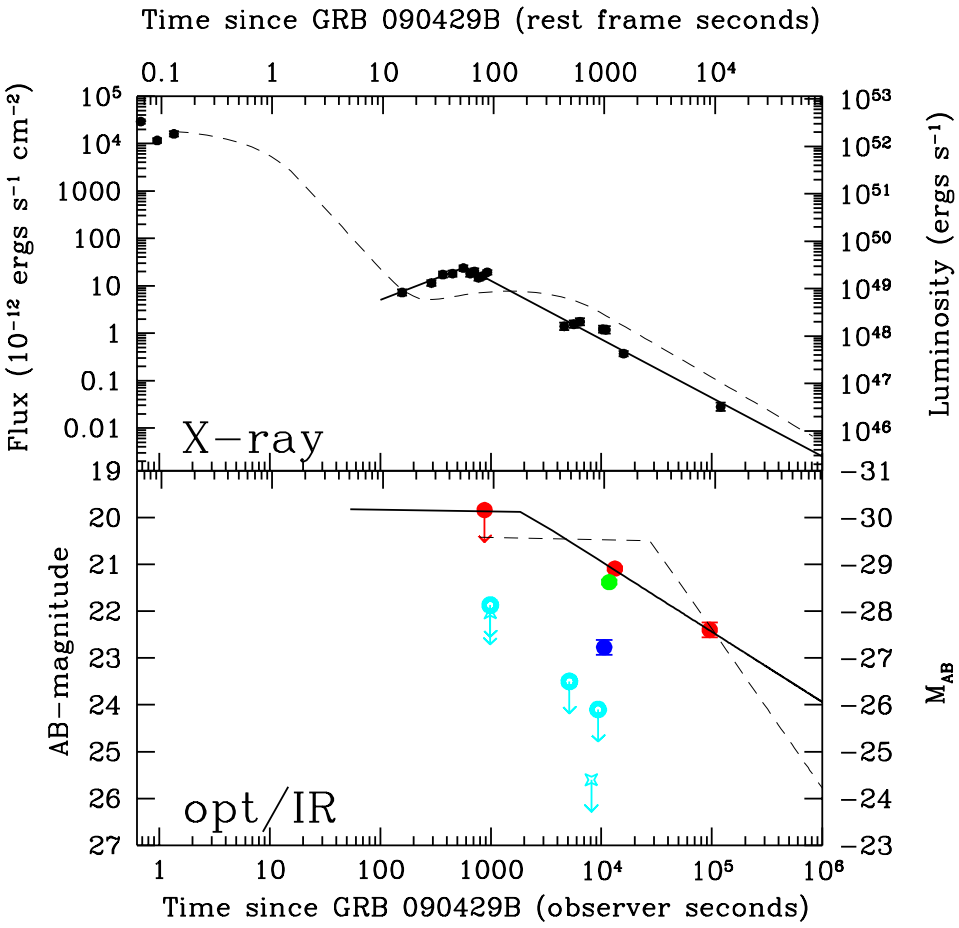

Fig. 1.— The X-ray (top) and optical/IR (bottom) lightcurve of GRB 090429B, the left hand and bottom axis represent the observed time and flux/magnitude, while the top and right hand axis show rest-frame time, and luminosity respectively. The solid points in the top panel show the observed XRT data, along with a solid line representing the model. The dashed line represents the best fit model for GRB 090423 (**?**) overplotted as it would appear at $z \sim 9.4$. The lower panel shows the optical lightcurve, along with a single power-law fit to the (red) K-band points. (H and J are shown as green and blue, respectively. For clarity we have shown only the i and z-band limits (cyan) in the optical). Additionally, the dashed line again shows the model of GRB 090423 at $z \sim 9.4$. As can be seen, the luminosity and general behaviour of GRB 090429B in both X-ray and optical is similar to that of GRB 090423.

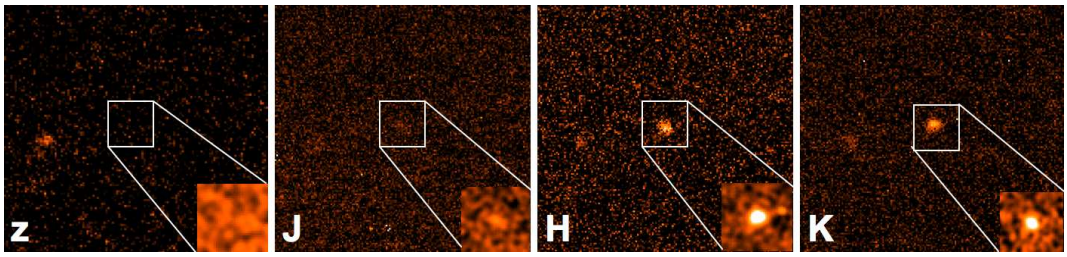

Fig. 2.— Discovery images of the GRB 090429B afterglow. The images are all obtained from Gemini-N, and show the deep non-detection in the z-band (which agrees with similar observations in $griz$ obtained at GROND, B,R,Z obtained at the VLT, and an i-band image at Gemini), coupled with the relatively bright object seen in H and K. At $z \sim 9.4$, Lyα lies within the J-band, and explains the marginal detection at that wavelength.

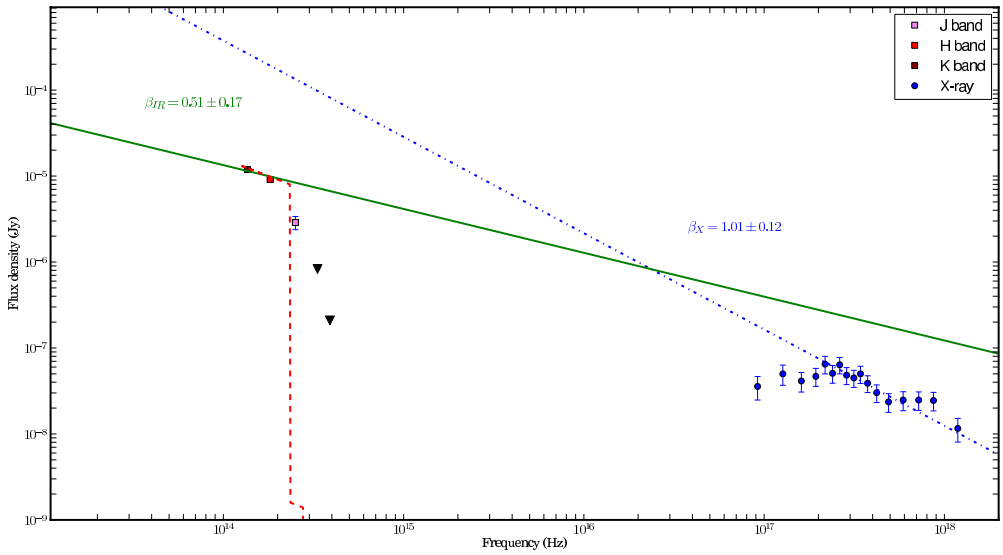

Fig. 3.— The IR to X-ray spectral energy distribution at $T_0 + 10^4$ s can be explained by an intrinsic broken power-law spectrum. The green solid line extends the IR spectral slope derived from the fit to the optical/NIR data, albeit that the prior on β_O does essentially fix this value. The blue dot-dashed line extrapolates the unabsorbed X-ray spectrum to lower frequencies, showing that a single power-law fails to fit the broadband SED at this time. The red dashed line shows the SED for the best-fit extreme-redshift ($z \sim 9.4$) model. z' and i' upper limits are shown as black triangles.

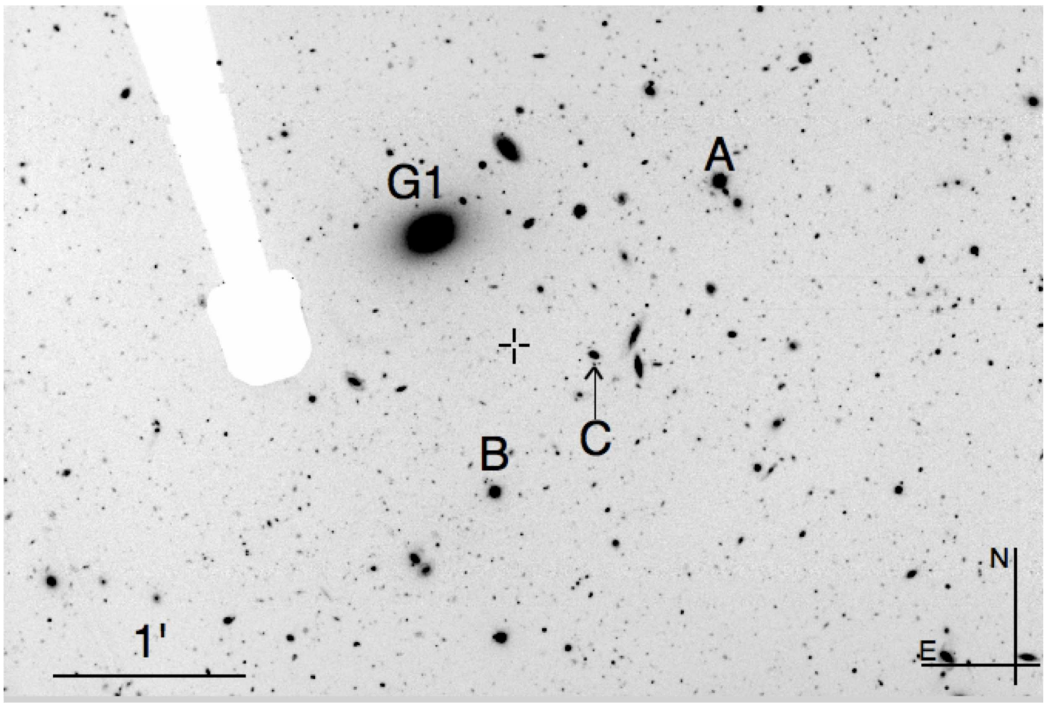

Fig. 4.— A wide field image of the GRB 090429B field, obtained with Gemini-N 14 days after the burst. The location of the GRB is marked with a crosshair. Additionally, we mark the positions of the three comparison stars used to refine our photometry (note that star C is faint, and lies at the end of the marked arrow, just to the south of the galaxy), and the location of a large elliptical galaxy (G1), which is the central galaxy of a modest cluster at $z \approx 0.08$, which may provide a modest lensing magnification. Note the silhouette of the guide probe obscures part of the field.

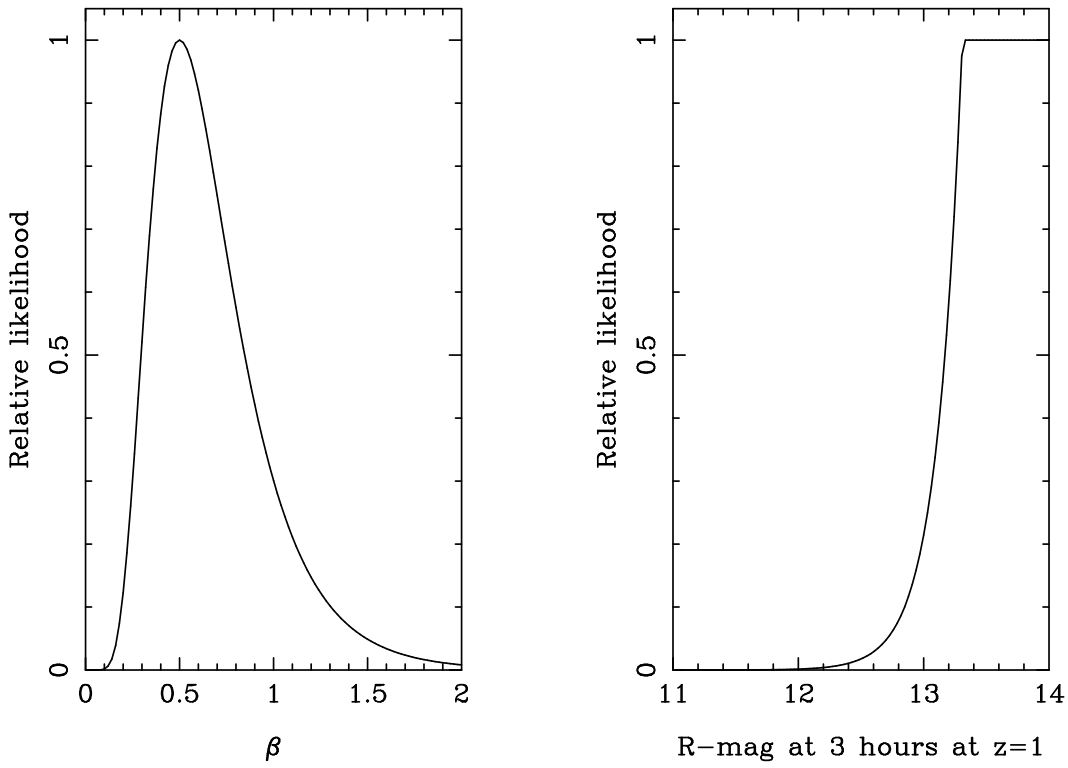

Fig. 5.— Input priors adopted for our photometric redshift fitting. [Left panel:] In the relativistic fireball model, the intrinsic spectral slope in the optical should lie between β_X and $\beta_X - 0.5$ (plus the associated measurement errors). To achieve this we use a lognormal distribution centred at 0.5 (since there does appear to be a break between the optical and X-ray, see Figure **??**). This is a relatively weak prior and simply avoids extreme values of β. [Right panel:] The second prior is on the intrinsic optical afterglow luminosity, and impacts solutions that would result in an unreasonably bright luminosity (it is not bounded at the faint end, and hence the low redshift solutions are unaffected). It is therefore based on the empirically observed upper envelope of afterglow luminosities. The primary impact of this prior is to disfavour moderate ($A_V > 3$) scenarios at high redshift ($z > 7$), where the burst would have been more luminous than any other known afterglow.

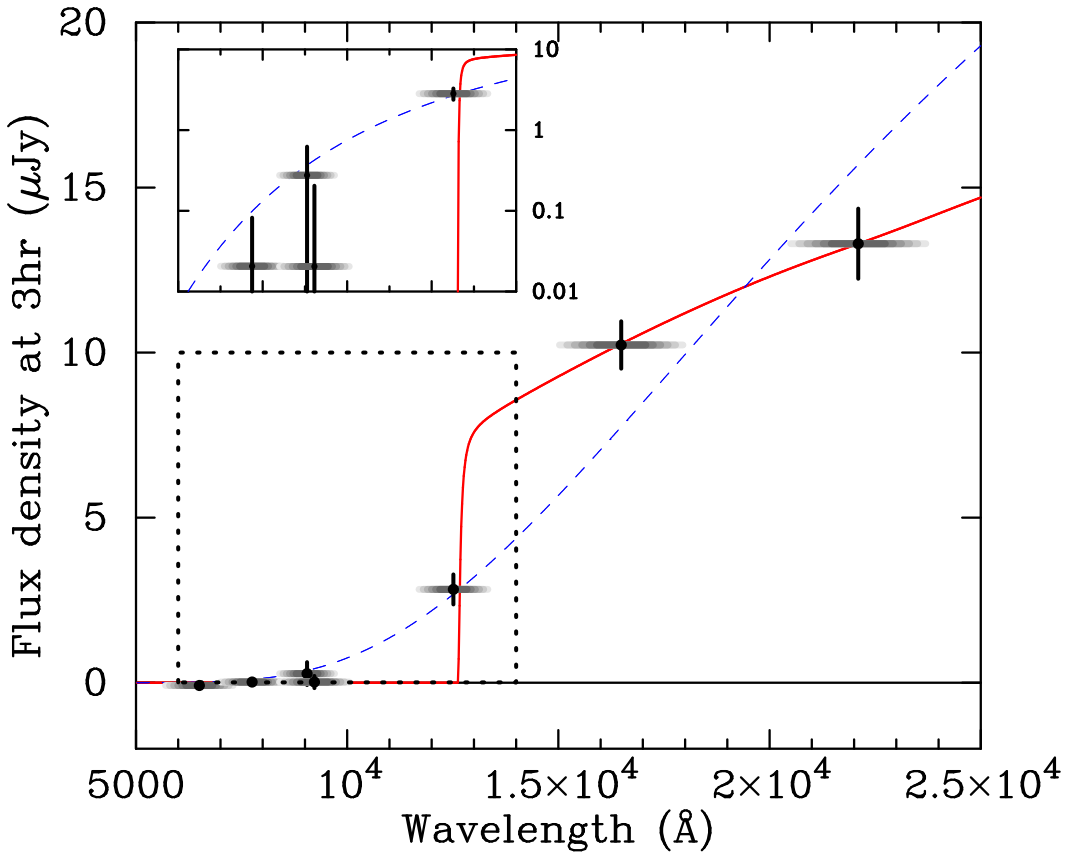

Fig. 6.— The spectral energy distribution of the GRB 090429B afterglow formed by extrapolating our observed photometry to 3 hours post-burst assuming the magnitude remains constant, i.e. $\alpha = 0$ (for varying α fits see Figure **??**). The vertical error bars represent 1σ uncertainty, and the horizontal shaded bars illustrate the widths of the broadband filters. The best fit model ($\chi^2/dof = 1.76/3$) to the data points is shown as the solid red line, the parameters being redshift $z = 9.36$, rest-frame extinction $A_V = 0.10$ and intrinsic power-law slope $\beta = 0.51$. The inset simply replots the short wavelength part of the figure (indicated by a dotted box) on a logarithmic flux density scale, to more clearly show the constraints from the optical measurements. An alternative low-redshift ($z \approx 0$), high extinction ($A_V = 10.6$) model is shown as a dashed blue line, but in fact is formally ruled out at high significance ($\chi^2/dof = 26.2/4$).

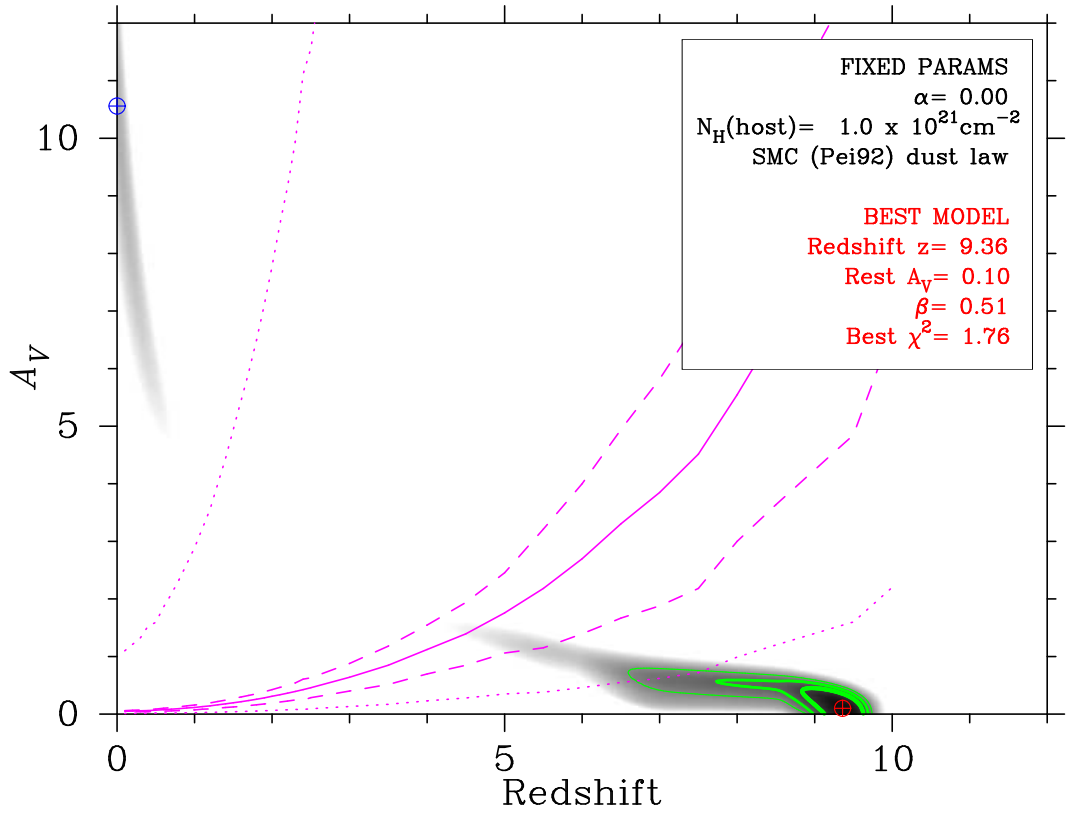

Fig. 7.— Confidence contours on a parameter space of redshift and host galaxy extinction for the GRB 090429B afterglow, for our favoured set of prior assumptions (green contours are 90%, 99% and 99.9% confidence). All fits at $z < 7.7$ are ruled out at $> 99\%$ confidence, and while fits can be found at $z \sim 0$ they are markedly worse than the high$-z$ solutions. The best low-z solution (formally at $z = 0$) is marked with the blue cross and requires $A_V \sim 10$, and is also disfavoured by the lack of any host galaxy to deep limits, and the inconsistency of the required A_V with the hydrogen column density measured from the X-ray afterglow. To illustrate this the best fit N_H from the X-ray spectrum is converted into A_V and plotted onto the contour plot as the purple lines (dashed lines show the 90% error range, and the dotted lines show the limits of the systematic error due spanning the range of gas-to-dust ratios reported by **?**). As can be seen the A_V inferred from the X-ray, and that required from the photometric redshift fit are inconsistent at low redshift, but broadly consistent with the high-z fit.

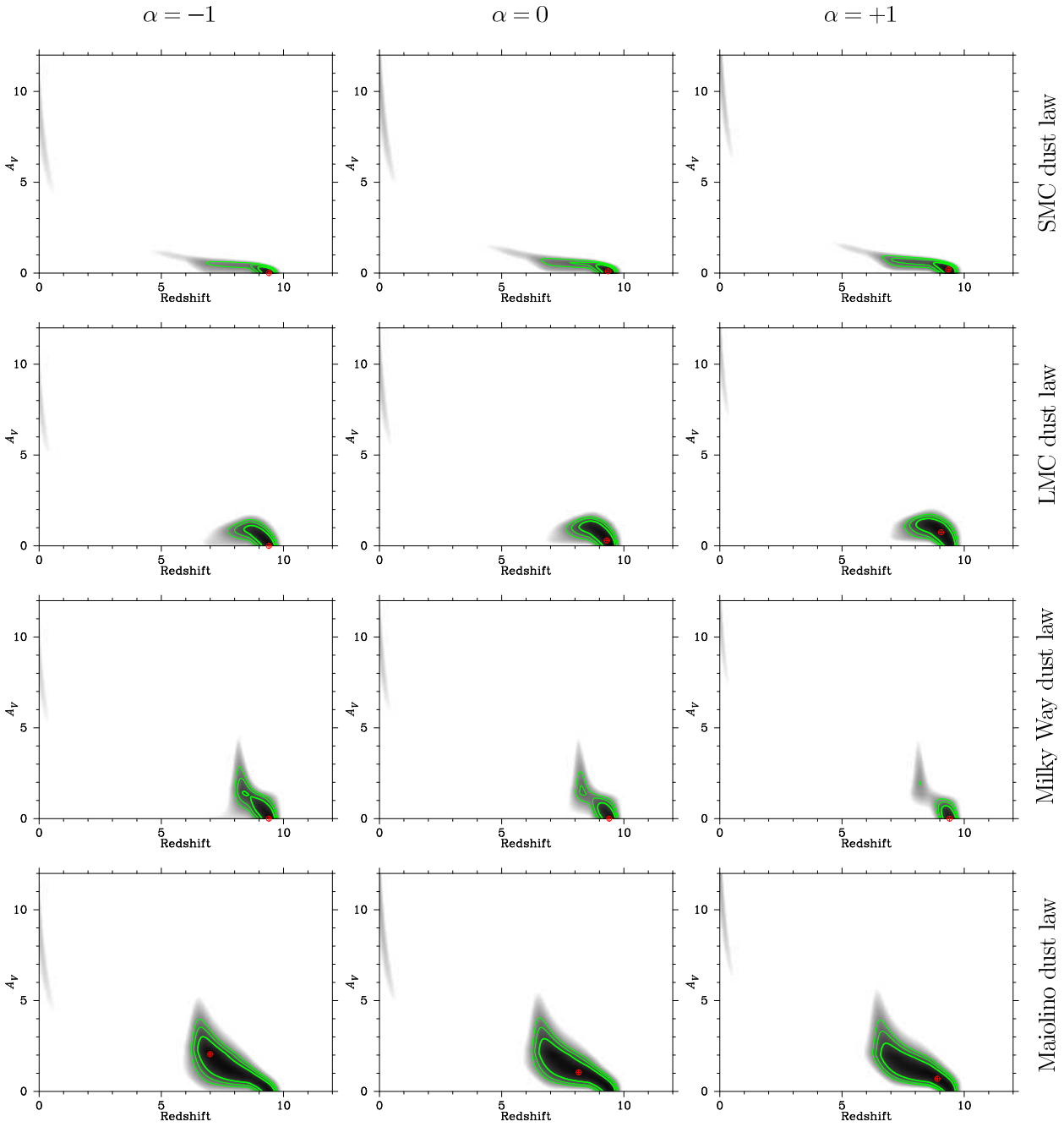

Fig. 8.— The results of SED fits with a range of possible values for the temporal power-law index, and different reddening laws. The plots encompass the canonical reddening laws for the SMC, LMC and Milky Way (which are characterized by the increasing influence of the 2175 Å bump) as well as the law of **?** which is approximately flat ("gray") from $\sim 1800 - 3000$ Å. As can be seen, the assumed temporal index has only a minimal impact on our results, and our assumption of $\alpha = 0$ therefore does not affect our analysis. The majority of GRB afterglows are best fit with SMC-like absorption, and we therefore adopt this as our choice model (e.g. **?**). Other laws can produce broader allowed redshift ranges, in particular extending as low as $z \sim 6.3$ at 99% confidence in the **?** case, but all rule out low-z scenarios.

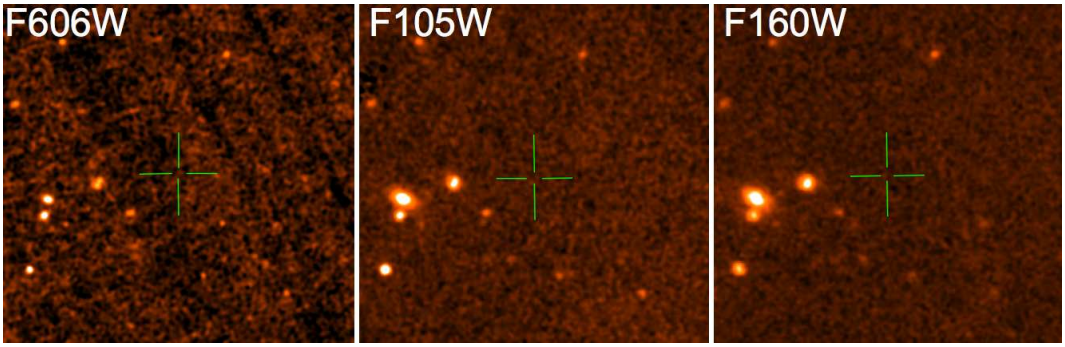

Fig. 9.— Our late time *HST* observations of the GRB 090429B field in the optical and NIR. No host galaxy is detected in any filter, supporting a high redshift origin, since a host with $z < 1$ would be very unlikely to be fainter than these limits, even if dusty. At F160W the host remains undetected, but the observations reach limits which would uncover $\sim 50\%$ of the $z > 8$ candidates in the Hubble Ultra-Deep Field (UDF). Hence, the non-detection of any host is fully consistent with our high-z model, but inconsistent with any lower redshift, high extinction scenario.

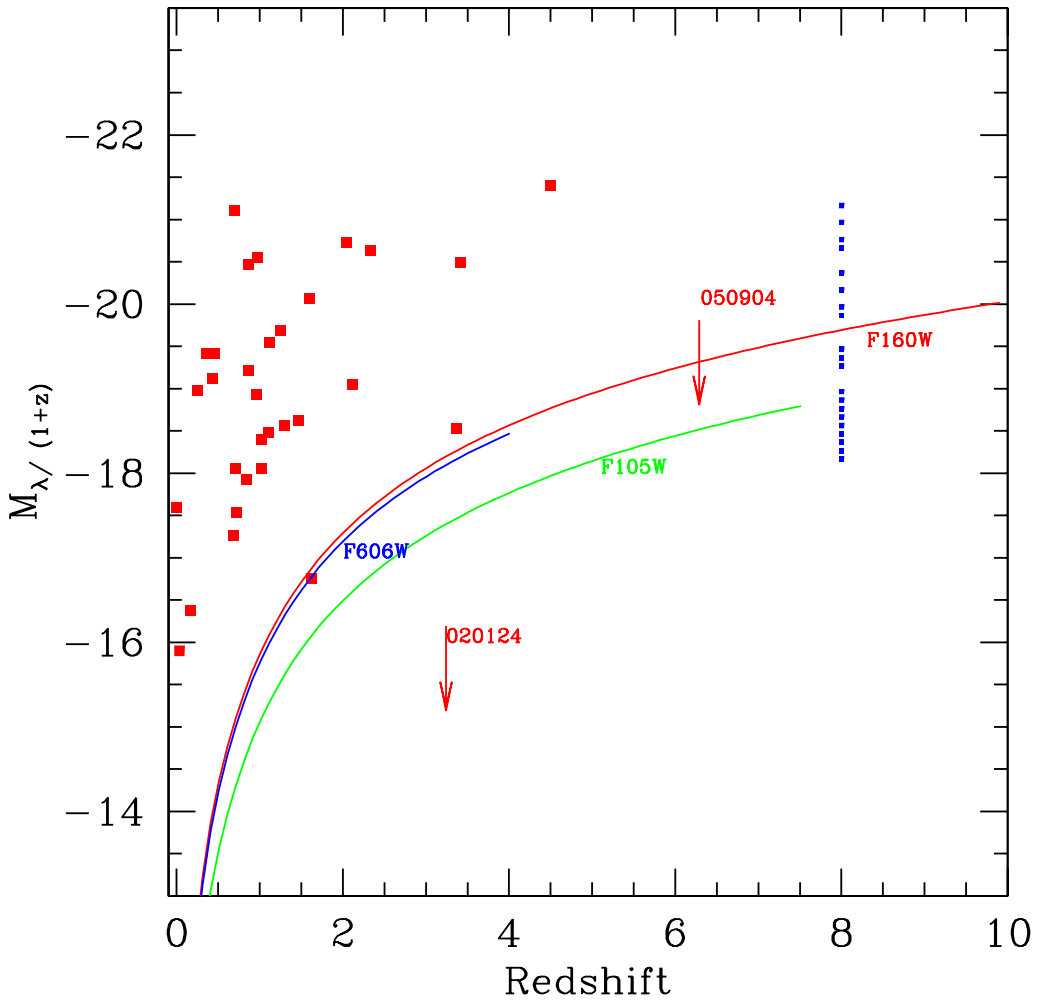

Fig. 10.— The solid lines show the 3σ absolute magnitude limits for GRB 090429B in each of our filters F606W (blue), F105W (green) and F160W (red). The inferred absolute magnitudes (AB) of a sample of GRB host galaxies (**?**), as a function of redshift (plot modified from **?**). The known GRB hosts with HST observations are plotted as red points, and are supplemented at high redshift by the observations of GRB 050904 by **?**. As can be seen, all of these lines lie significantly below the majority of GRB hosts and offer support for a high redshift origin for GRB 090429B. The blue points at $z \sim 8$ represents the Lyman break sample of **?**. As can be seen, the limiting magnitude for GRB 090429B lies roughly at the median of this distribution, and so the non-detection in our observations would not be unexpected at $z \sim 9.4$